Sixth International Symposium on Turbulence and Shear Flow Phenomena
Seoul, Korea, 22-24 June 2009

# Direct numerical simulations of canonical shock/turbulence interaction

**Johan Larsson**
Center for Turbulence Research, Stanford University
Stanford, CA 94305-3035, USA
jola@stanford.edu

**Sanjiva K. Lele**
Department of Aeronautics and Astronautics, Stanford University
Stanford, CA 94305-4035, USA
lele@stanford.edu

## ABSTRACT

A set of direct numerical simulations of isotropic turbulence passing through a nominally normal shock wave are presented. Upstream of the shock, the microscale Reynolds number is 40, the mean Mach number is 1.3–6.0, and the turbulence Mach number is 0.22. It is shown that the Kolmogorov scale decreases during the shock-interaction, which implies that the grid resolution needed to resolve the viscous dissipation is finer than used in previous studies. This leads to some qualitative differences with previous work, e.g. that the streamwise vorticity variance increases rapidly behind the shock.

## MOTIVATION AND OBJECTIVES

Shock/turbulence interaction is a fundamental phenomenon in fluid mechanics that occurs in a wide range of interesting problems in various disciplines of science. Examples include supernovae explosions, inertial confinement fusion, hypersonic flight and propulsion, and shock wave lithotripsy (used to break up kidney stones). In many such applications the shock/turbulence interaction includes additional complexities, e.g., real gas effects, multiple species, non-uniform mean flow, or streamline curvature. The most fundamental problem, where these additional complexities have been removed, is arguably that of isotropic turbulence passing through a nominally normal shock wave in a perfect gas. Given the historical success in studying building-block problems in fluid mechanics, canonical shock/turbulence interaction is the focus of the present study.

Ribner (1954) studied the problem analytically by solving the linearized Euler equations with linearized shock jump conditions for incoming purely vortical turbulence. This linear interaction analysis (LIA) relies on several assumptions, most notably that the turbulence comprises a small perturbation relative to the shock and that nonlinear effects in the post-shock evolution are small (as well as the standard assumption of a difference in time scales). Rapid distortion theory (RDT) relies on the same assumptions, but additionally neglects both the post-shock linear evolution and all effects of the turbulence on the shock. In addition, the Rankine-Hugoniot shock jump conditions are incorporated into LIA but not RDT; one consequence is that LIA captures the generation of sound and entropy waves from incoming purely vortical turbulence.

Lee *et al.* performed a set of landmark direct numerical simulations (DNS) of canonical shock/turbulence interaction in a sequence of papers (Lee *et al.*, 1993, 1997). The first of these papers considered shocks at Mach numbers up to 1.2 where the viscous structure of the shock was resolved; these were therefore truly direct solutions of the Navier-Stokes equations. In the second paper they verified that these "true" DNS results at Mach 1.2 could be replicated by instead capturing the shock (at considerably lower cost), provided sufficient grid resolution in the shock-normal direction at the shock. This methodology was then used to compute cases at Mach numbers up to 3. When comparing the results to LIA predictions, they found that LIA realistically represents many features, including the amplification of transverse vorticity, the amplification and post-shock evolution of the Reynolds stresses, and the decrease in transverse Taylor length scale.

Mahesh *et al.* (1997) considered the influence of entropy fluctuations in the upstream turbulence, and found that negatively correlated velocity and temperature fluctuations lead to enhanced amplifications of turbulence kinetic energy and vorticity. Later, Jamme *et al.* (2002) resolved the viscous shock structure at Mach 1.2 and 1.5, and essentially confirmed the findings of Mahesh *et al.*. Barre *et al.* (1996) studied the problem experimentally in a windtunnel, and measured velocity variances using hot-wires and LDV.

The present study builds on these previous studies, especially those by Lee *et al.* (1993, 1997) (henceforth refered to as Lee93 and Lee97, respectively). In this paper, DNS in the extended sense of capturing the shock while directly resolving all scales of turbulence is used. It will be shown that a simple argument about the Kolmogorov scale implies that DNS requires a refined grid in both the shock-normal *and* the transverse directions to fully resolve the viscous scales of turbulence. This is verified by a grid convergence study, and implies that the calculations in the studies mentioned above were, most likely, under-resolved. The present DNS data is fully resolved, which leads to larger differences between the data and LIA. The Reynolds stresses are more anisotropic in the present DNS, and there are qualitative differences in the Taylor length scales. Moreover, the vorticity components return to isotropy in all cases in the present study. This raises the interesting question of whether under-resolution of the post-shock turbulence in DNS essentially neglects some phenomenon that is also neglected in the LIA. This will be explored below.

Throughout this paper the subscripts "u" and "d" refer to average states upstream and downstream of the shock, respectively. For quantities that evolve in the streamwise direction, these states are obtained by extrapolation to the average shock location. The mean flow and tur-

bulent Mach numbers are defined as $M = u_{1,\mathrm{u}}/c_\mathrm{u}$ and $M_t = \sqrt{\langle u_i' u_i' \rangle_\mathrm{u}}/c_\mathrm{u}$, respectively, where $u_1$ is the velocity in the streamwise (shock-normal) direction and $c$ is the speed of sound. All cases discussed here have $M_t \approx 0.22$ immediately upstream of the shock.

## NUMERICAL METHOD

The compressible Navier-Stokes equations for a perfect gas with ratio of specific heats $\gamma = 1.4$ are solved using a solution-adaptive finite difference method (Larsson *et al.*, 2007). Near shocks, a fifth-order accurate weighted essentially non-oscillatory (WENO) scheme is used to approximate the inviscid fluxes, whereas a sixth-order accurate central difference scheme on the split form by Ducros *et al.* (2000) is used in the remainder of the domain. The sensor $s = -\theta/(|\theta| + \sqrt{\langle \omega_j \omega_j \rangle_{yz}})$ is used to identify regions of shock waves at every time step, where $\theta = \partial_j u_j$ is the dilatation, $\omega_i = \epsilon_{ijk}\partial_j u_k$ is the vorticity, and $\langle\cdot\rangle_{yz}$ is an average over the transverse directions to avoid spuriously high sensor-values at grid points with small vorticity. The WENO scheme is applied in regions of $s > 0.5$. Note that the WENO scheme is applied in all directions, which was found necessary for stable calculations at high values of $M_t$. This solution-adaptivity leads to a method that captures the shocks in a crisp and accurate fashion while introducing only minimal amounts of numerical dissipation. This has been shown to lead to a broad range of well-resolved scales (Larsson *et al.*, 2007). The viscosity is assumed to follow the power-law $\mu = \mu_\mathrm{ref}\,(T/T_\mathrm{ref})^{3/4}$, and the Prandtl number is taken as $Pr = 0.7$. The viscous terms are treated by a sixth-order accurate central scheme, and the system is integrated in time using a fourth-order accurate Runge-Kutta method. The solution-adaptive method introduces internal interfaces between the central and WENO schemes; these are treated in a way similar to that devised by Pirozzoli (2002) to ensure conservation of mass, momentum and total energy. The numerical stability of these internal interfaces was analyzed by Larsson & Gustafsson (2008), where it was shown that the full (coupled) method is linearly stable. Thus any spurious oscillations introduced by the solution-adaptive switching of schemes are bounded. The code has been thoroughly verified on several benchmark problems.

The computational domain is $4\pi \times (2\pi)^2$ in the streamwise and transverse directions. The grid is stretched in the streamwise direction such that the streamwise grid spacing at and behind the shock is approximately 3 times finer than the transverse spacing.

All computational studies necessarily involve various sources of error, and it is essential to analyze and quantify their impact. This is especially true for canonical shock/turbulence interaction, which despite its geometrical simplicity has some very subtle potential sources of error. In the following subsections we consider those elements of the problem that have the largest influence on the accuracy of the results.

### Inflow turbulence

It is important to ensure that the turbulence immediately upstream of the shock is realistic, fully developed and well-characterized. In the present study the inflow turbulence is generated in several steps to meet these criteria, essentially following the technique proposed by Xiong *et al.* (2004). First, several independent but statistically identical fields of isotropic turbulence in periodic boxes are generated using the methodology proposed by Ristorcelli & Blaisdell (1997). These fields have exponentially decaying velocity spectra $E(k) \sim k^4 \exp\left(-2k^2/k_0^2\right)$, with peak energy at wavenumber $k_0 = 4$ and microscale Reynolds number $Re_\lambda = \rho\lambda\sqrt{\langle u_i' u_i' \rangle/3}/\mu = 140$, where $\lambda$ is the Taylor length scale. They are then allowed to decay temporally (i.e., in periodic boxes) for approximately three eddy turnover times $\lambda/\sqrt{\langle u_i' u_i' \rangle/3}$, which ensures that the turbulence is fully developed and realistic. These independent realizations are blended together into a longer inflow database, which is then used together with Taylor's hypothesis to specify the time-dependent inflow turbulence. This technique leads to very accurate spatially decaying turbulence immediately behind the inlet (Xiong *et al.*, 2004; Larsson, 2009). After the decay, the Reynolds number immediately upstream of the shock is $Re_\lambda \approx 40$. The thermodynamic quantities are approximately but not perfectly isentropic: immediately upstream of the shock the rms-values are $\rho'_{\mathrm{rms,u}}/(\rho_\mathrm{u} M_t^2) = 0.42 \pm 0.02$, $p'_{\mathrm{rms,u}}/(\gamma p_\mathrm{u} M_t^2) = 0.37 \pm 0.02$, and $T'_{\mathrm{rms,u}}/((\gamma-1)T_\mathrm{u} M_t^2) = 0.35 \pm 0.03$.

### Outflow boundary condition

The flow behind the shock is subsonic, and thus care must be taken not to generate acoustic reflections from the outflow boundary condition. This is accomplished through a sponge region that damps the solution toward a quiescent state before reaching the boundary. Terms of the form

$$-\sigma \left( \frac{x_1 - x_{1,\mathrm{sp}}}{x_{1,\max} - x_{1,\mathrm{sp}}} \right)^2 (f - \langle f \rangle_{yz})$$

are added to the Navier-Stokes equations, where $\sigma$ is a constant, $x_{1,\mathrm{sp}}$ is the beginning of the sponge region, $x_{1,\max}$ is the end of the domain, $f = \rho, \rho u_i, \rho e_0$ denotes each conserved variable, and $\langle\cdot\rangle_{yz}$ denotes an average in the transverse directions. We note that this form of the sponge terms does not require knowledge of the average state at the outlet. The length of the sponge region is $x_{1,\max} - x_{1,\mathrm{sp}} = \pi$.

The issue of avoiding acoustic reflections from an outflow is common in the literature; however, the more interesting issue is instead that of specifying the mean back pressure $p_\infty$ (applied at the outflow boundary) such that the shock is stationary in the mean. Consider first a shock in a laminar flow with conditions $u_{1,\mathrm{u}}$ and $p_\mathrm{u}$ upstream of the shock, $p_\mathrm{d}$ downstream of the shock, and $p_\infty$ at the outlet boundary. Assume that the shock is moving toward the outlet at a speed $\langle U_s \rangle$. The Rankine-Hugoniot relation for the pressure jump then becomes

$$\frac{p_\mathrm{d}}{p_\mathrm{u}} = 1 + \frac{2\gamma}{\gamma+1}\left[ \frac{(u_{1,\mathrm{u}} - \langle U_s \rangle)^2}{c_\mathrm{u}^2} - 1 \right], \qquad (1)$$

and $p_\infty = p_\mathrm{d}$. For this laminar case it is straightforward to specify the back pressure $p_\infty$ such that the shock is stationary. In a turbulent flow, however, the Rankine-Hugoniot relation (1) is only valid instantaneously and not on average. Lele (1992) used RDT to develop approximate shock relations for turbulent flow, and found that the density and pressure jumps decrease in the presence of turbulence for a given shock Mach number. Furthermore, the viscous decay of turbulence kinetic energy behind the shock causes a spatially increasing internal energy, and hence $p_\infty \neq p_\mathrm{d}$. Given these complications, it is clearly difficult to specify *a priori* the back pressure that yields a stationary shock.

In the present study we therefore proceed by first computing each case on a coarse grid with back pressure

$p_{\infty,\mathrm{initial}}$ given by the laminar Rankine-Hugoniot conditions, and computing the resulting average shock-speed $\langle U_s\rangle_{\mathrm{initial}}$. Differentiation of (1) with respect to $p_\mathrm{d}$ and $\langle U_s\rangle$ gives a relation between small changes $\Delta p_\mathrm{d}$ and $\Delta\langle U_s\rangle$. Further assuming that $\Delta p_\infty \approx \Delta p_\mathrm{d}$ (i.e., that the viscous decay of kinetic energy is unaffected by changes in the shock-speed) gives the relation

$$\Delta p_\infty \approx \frac{-4\rho_\mathrm{u} u_{1,\mathrm{u}}}{\gamma+1}\Delta\langle U_s\rangle\,. \tag{2}$$

After finding the initial shock-speed $\langle U_s\rangle_{\mathrm{initial}}$, this relation is used to adjust the back pressure as $p_\infty = p_{\infty,\mathrm{initial}} + \Delta p_\infty \approx p_{\infty,\mathrm{initial}} + (4\rho_\mathrm{u} u_{1,\mathrm{u}}/(\gamma+1))\,\langle U_s\rangle_{\mathrm{initial}}$.

In practice the initial shock-speed is close to zero at low turbulence intensities, but can be almost 1% of the upstream velocity at the highest turbulence intensities considered here. With the adjustment to $p_\infty$ given by Eq. (2), the resulting average shock-speed is $|\langle U_s\rangle|/u_{1,\mathrm{u}} < 0.0002$ for all cases in the present study.

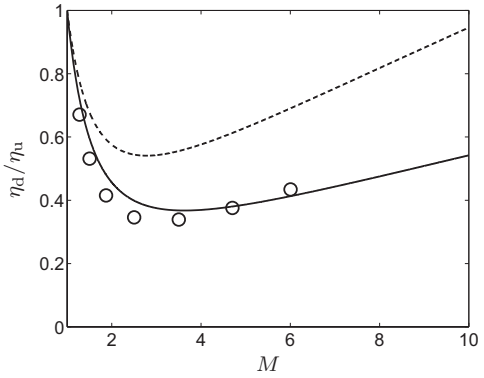


Figure 1: Change in the Kolmogorov scale across the shock as a function of Mach number. Estimate from Eq. (3) in lines with $\gamma = 1.4$ (solid) and $\gamma = 5/3$ (dashed). Results from DNS in symbols.

#### Grid sensitivity

Direct numerical simulation of turbulence requires that the viscous dissipation is fully resolved. Denoting the maximum resolved wavenumber as $k_\mathrm{max}$, this typically requires (Pope, 2000) $k_\mathrm{max}\eta \gtrsim 1.5$, where $\eta = \left(\nu^3/(\varepsilon/\rho)\right)^{1/4}$ is the Kolmogorov length scale (using the incompressible definition) and $\nu$ and $\varepsilon$ are the kinematic viscosity and rate of dissipation of kinetic energy, respectively. This estimate is applicable to isotropic turbulence, or possibly turbulence that is only locally isotropic (i.e., isotropic at the smallest scales). The turbulence in canonical shock/turbulence interaction is isotropic upstream of the shock, and axisymmetric and out of equilibrium immediately downstream of the shock. It is not clear *a priori* whether the turbulence returns to isotropy. The present DNS data shows that the vorticity components become isotropic at $k_0 x_1 \approx 10$, whereas the Reynolds stresses stay anisotropic (axisymmetric) throughout the domain (discussed below; shown in Figs. 4(c) and 6(b)). Given that vorticity is primarily associated with small-scale motions, one could argue that the concept of the Kolmogorov scale and its relation to the grid resolution makes sense upstream of the shock ($x_1 < 0$) and for $k_0 x_1 \gtrsim 10$. A first assessment of the necessary grid resolution is done by considering the requirement $k_\mathrm{max}\eta \gtrsim 1.5$ in these regions.

Consider the approximate scaling of the Kolmogorov length scale

$$\eta = \left(\frac{\nu^3}{\varepsilon/\rho}\right)^{1/4} \sim \left(\frac{\mu^2}{\rho^2\omega^2}\right)^{1/4} \sim \frac{T^{3/8}}{\rho^{1/2}\,\omega^{1/2}}\,,$$

where the relations $\varepsilon \approx \mu\omega^2$, $\nu = \mu/\rho$, and $\mu \sim T^{3/4}$ have been used. The streamwise and transverse vorticity components change differently at the shock. Taking the (larger) transverse components, and assuming that these change as the density jump (the RDT result), gives $\omega_{2,\mathrm{d}}/\omega_\mathrm{u} \sim \rho_\mathrm{d}/\rho_\mathrm{u}$. This yields the change at the shock as

$$\frac{\eta_\mathrm{d}}{\eta_\mathrm{u}} \approx \left(\frac{T_\mathrm{d}}{T_\mathrm{u}}\right)^{3/8}\left(\frac{\rho_\mathrm{d}}{\rho_\mathrm{u}}\right)^{-1}\,, \tag{3}$$

where the jumps in temperature and density can be inserted from the Rankine-Hugoniot relations. This is shown in Fig. 1, where it is clear that the Kolmogorov scale decreases across the shock. Also shown in the figure are the results from the present DNS; despite the somewhat crude estimate, the DNS agrees with the prediction with surprising accuracy. Specifically, the DNS data both confirm the quantitative decrease in the Kolmogorov scale, and the qualitative effect of increasing $\eta_\mathrm{d}/\eta_\mathrm{u}$ for $M \gtrsim 3$. The latter is due to the saturation of the density jump; the temperature dependence $(T_\mathrm{d}/T_\mathrm{u})^{3/8}$ is essentially linear.

This estimated change in the Kolmogorov scale is not unexpected given the compressive nature of a shock, but, more importantly (at this stage), it has an effect on the necessary grid resolution. The present study uses grids that are refined in the streamwise direction, implying that the critical resolution is in the transverse directions. Therefore resolution of the post-shock viscous dissipation requires 2.5 times as many grid points as resolving the pre-shock dissipation – in *every* direction.

Now, this estimate is both approximate and only valid for $k_0 x_1 \gtrsim 10$. In the region immediately behind the shock ($0 \le k_0 x_1 \lesssim 10$) the turbulence is out of equilibrium, and the length scale of viscous dissipation is not well defined. A simple argument (the RDT result) is that the turbulence is compressed only in the streamwise direction behind the shock, which suggests that streamwise grid refinement is sufficient there. This is the reason for using grids with approximately 3 times finer grid spacing in the streamwise direction both *at* the shock and *behind* it.

The true test of whether the grid is sufficiently fine is a systematic grid refinement. Fig. 2 shows a sample result from such a grid refinement study, in this case the vorticity variances for a case with $M = 1.9$ on successively refined grids. We note that vorticity is a sensitive quantity (given its dependence on small scales), and that other quantities converge more quickly. The figure shows that there is convergence. A close inspection reveals that the maximum difference between the two finest grids is 2%, which serves as an error estimate for the vorticity variances; quantities that depend more on the large-scale motions have lower errors. Also note that the vorticity components fail to return to isotropy on the coarsest grids, where the post-shock turbulence is under-resolved.

In conclusion, the results are statistically converged to within 2% on the finest grid with $1040 \times 384^2 \approx 153 \cdot 10^6$ grid points. The fact that such a fine grid is needed even for a relatively low $Re_\lambda \approx 40$ is due to the change in the Kolmogorov scale at the shock. It will be shown below that the Taylor length scales and vorticity variances behave dif-

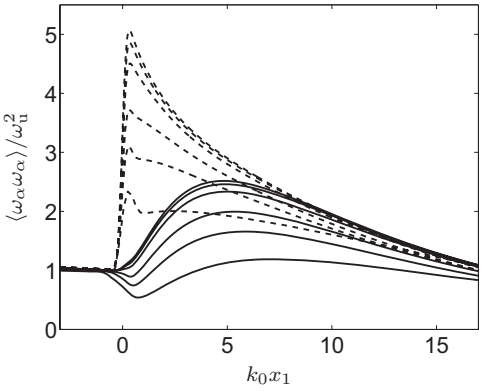


Figure 2: Convergence of streamwise (solid) and transverse (dashed) vorticity variances under grid refinement for Mach 1.9. Grids with $174\times64^2$, $261\times96^2$, $347\times128^2$, $521\times192^2$, $694\times256^2$, and $1040\times384^2$ points, where finer grids yield higher variances.

ferently in the present data compared to that of Lee97; this difference is most likely due to the better resolution of the post-shock turbulence.

## AVERAGE RESULTS

Once the initial transients have disappeared, averages are collected over the transverse directions and a period of time $k_0\,u_{1,\mathrm{u}}\,t_\mathrm{stats}\approx 100$. The computed averages change little when decreasing the averaging period by half, thus confirming that the averages are converged.

There are many possible ways to non-dimensionalize the streamwise coordinate, both by turbulence length scales and convected turbulence time scales (e.g., collapsing the decay). Here we choose to scale the streamwise coordinate by the wavenumber of peak energy $k_0$ in order to facilitate comparison with linear analysis. In all figures the streamwise coordinate has been shifted such that the average position of the shock is at $x_1=0$. With this shift, the inflow is at $k_0x_1\approx-8$, the outflow is at $k_0x_1\approx42$ and the sponge region begins at $k_0x_1\approx30$. The transverse domain size is $k_0L_{2,3}=8\pi$.

### Mean profiles

The mean profiles of density are shown in Fig. 3 for a selection of Mach numbers. The jumps at the shock are consistently smaller than the laminar Rankine-Hugoniot relations, and the relative deviations from the laminar jumps increase for lower Mach numbers. This is to be expected, since the turbulent $M_t$ is held constant; thus the turbulence intensity is higher at lower $M$. The profiles of density (and pressure, though not shown) show the same qualitative structure: first the jump at the shock, then a small decrease, and finally a slow increase toward the outflow. The slow increase toward the outflow is sensitive to the exact implementation of the downstream boundary condition. In the present study, non-reflecting boundary conditions based on a linearization around the laminar post-shock state are used, which may explain why all profiles approach the laminar state downstream. Therefore, the downstream development of the mean quantities should not be taken as the truth. Disregarding the downstream development, all profiles still show an overshoot immediately behind the shock. Thus, on average, there is a compression at the shock followed by a slight expansion.

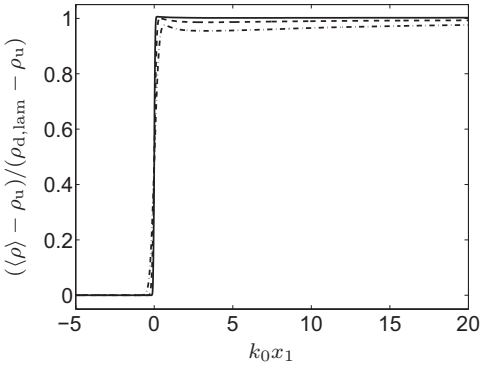


Figure 3: Mean density, scaled with laminar post-shock density $\rho_\mathrm{d,lam}$. Mean Mach numbers 6.0 (solid), 2.5 (dashed), and 1.5 (dash-dotted).

The deviation from the laminar shock jumps was analyzed by Lele (1992), who derived the turbulent jump conditions and used RDT to approximately close them. Lele's theory is qualitatively consistent with the present results in that turbulence leads to decreased jumps in mean density and pressure.

### Velocity variances

The velocity variances are shown in Fig. 4 for the same selection of cases. The transverse Reynolds stress $\langle u_2'u_2'\rangle$ increases at the shock followed by monotonic decay. The streamwise stress $\langle u_1'u_1'\rangle$ has a large peak at the mean shock location due to the unsteady shock motion, and then evolves non-monotonically. This evolution is captured in linear analysis, and is due to a transfer of energy from acoustical to vortical modes behind the shock (cf. Lee97).

The anisotropy of the Reynolds stresses $\langle u_1'u_1'\rangle/\langle u_2'u_2'\rangle$ is shown in Fig. 4(c), where it is clear that the shock-interaction causes the turbulence to become anisotropic. The post-shock anisotropy as quantified by $\langle u_1'u_1'\rangle/\langle u_2'u_2'\rangle$ is between 1.2 to 1.4 depending on Mach number. There is no real evidence of a return-to-isotropy in the numerical results, implying that this process, if present, is significantly slower than the viscous decay. Comparison to the results by Lee97 shows a somewhat faster adjustment behind the shock, which is either due to the fully developed upstream turbulence in the present study having more fine-scale features (with shorter length/time scales) or an effect of insufficient post-shock resolution in their results.

The amplification of the far-field Reynolds stresses versus $M$ is shown in Fig. 5, where it is compared to the prediction of linear interaction analysis (LIA, taken from Lee97), the results of Lee97, and the experiments by Barre *et al.* (1996). The present DNS data agree very well with LIA for the trace $\langle u_j'u_j'\rangle$, but yield much larger anisotropy for all Mach numbers. Specifically, $\langle u_1'u_1'\rangle > \langle u_2'u_2'\rangle$ for all present cases. This agrees qualitatively with the experiment by Barre *et al.*, but contradicts both LIA and the results of Lee97 (both of which predict higher transverse stress for $M\gtrsim2$). The logical interpretation is that nonlinear effects must be important in the post-shock evolution; these are excluded from LIA and underpredicted when failing to fully resolve the post-shock turbulence.

### Vorticity variances

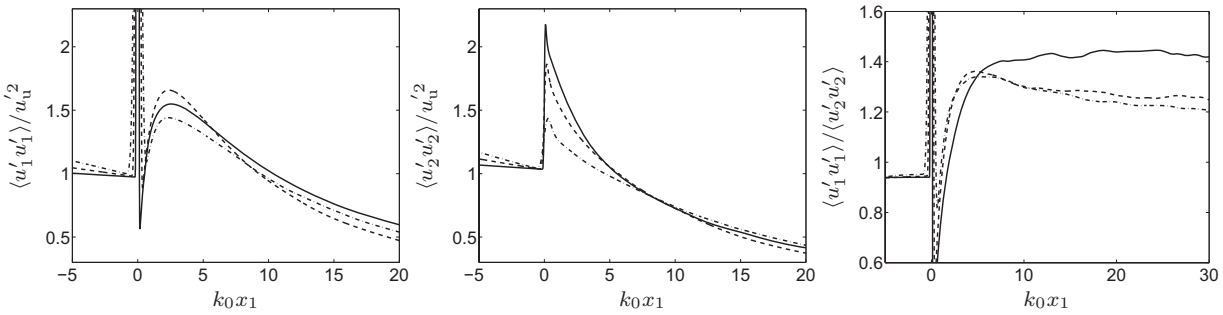


(a) Streamwise. (b) Transverse. (c) Anisotropy.

Figure 4: Velocity variances. Mean Mach numbers 6.0 (solid), 2.5 (dashed), and 1.5 (dash-dotted).

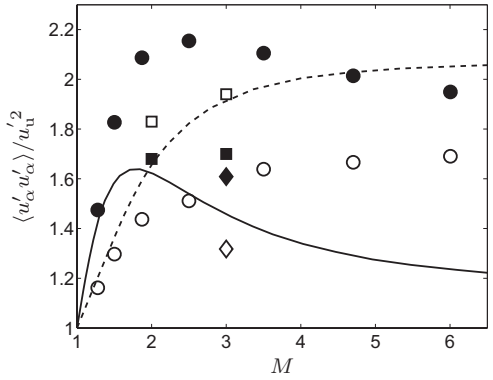


(a) Streamwise (solid line, filled symbols) and transverse (dashed line, open symbols) Reynolds stresses.

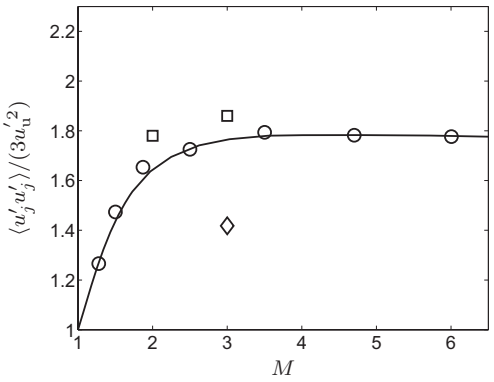


(b) Trace of Reynolds stress.

Figure 5: Amplification of Reynolds stresses from present DNS (circles), computations by Lee97 (squares), experiment by Barre *et al.* (diamonds), and LIA taken from Lee97 (lines). The results have been extrapolated from the far-field to the mean shock-location.

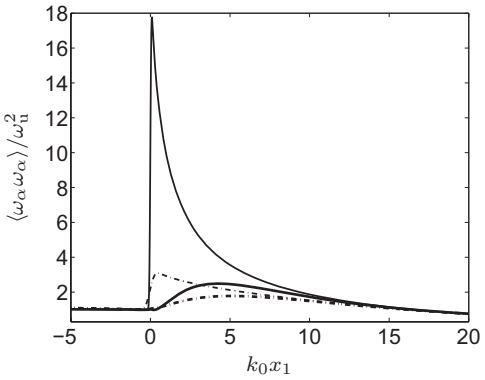


(a) Transverse (upper curves) and streamwise (lower curves) variances.

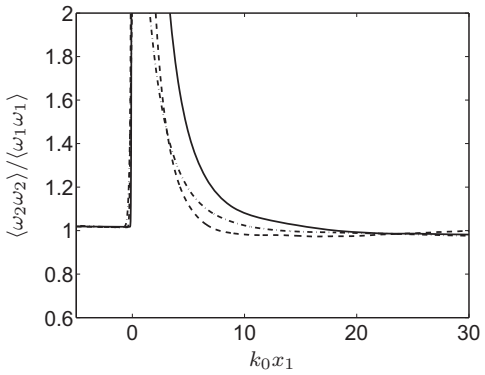


(b) Anisotropy.

Figure 6: Vorticity variances. Mean Mach numbers 6.0 (solid), 2.5 (dashed), and 1.5 (dash-dotted).

The vorticity variances are shown in Fig. 6 for a few cases. The transverse vorticity is amplified directly at the shock, and then decays. The streamwise vorticity is initially unaffected by the shock, but then quickly increases until it equilibrates with the transverse components. Fig. 6(b) shows that there is a clear return to (local) isotropy for the vorticity components at $k_0x_1 \approx 10$. This is in contrast to earlier work by Lee97, where the transverse vorticity was still 50% larger than the streamwise at $k_0x_1 \approx 12$ (the end of their domain). Again, the most plausible explanation is the grid resolution. It was shown in Fig. 2 that the vorticity components fail to return to isotropy when the post-shock turbulence is under-resolved. Since the post-shock vorticity evolution is a nonlinear process, where transverse vorticity is tilted into the streamwise direction, one can hypothesize that insufficient grid resolution inhibits this process.

#### Kolmogorov length scale

The evolution of the Kolmogorov length scale $\eta$ is shown in Fig. 7. Given that the turbulence is out of equilibrium (and locally anisotropic) for $k_0x_1 \lesssim 10$, it is not clear how one should interpret $\eta$ (computed from the isotropic definition) in this region. Nevertheless, the decrease at the shock is clear, as is the weakening of this effect for the highest Mach numbers. To compensate for the viscous growth, the post-shock Kolmogorov scale is computed by extrapolation to the mean shock position; these are the values shown in Fig. 1.

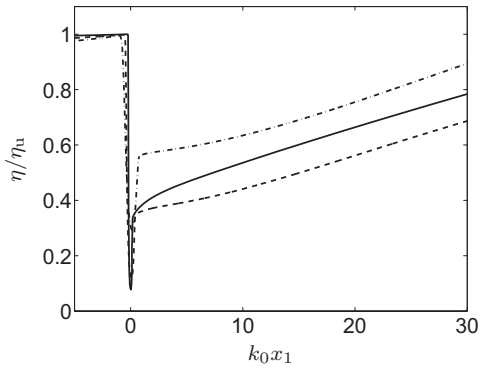


Figure 7: Kolmogorov length scale. Mean Mach numbers 6.0 (solid), 2.5 (dashed), and 1.5 (dash-dotted).

## SUMMARY AND CONCLUSIONS

A set of direct numerical simulations (DNS) of canonical shock/turbulence interaction is presented. Care is taken to ensure fully developed isotropic turbulence upstream of the shock, and a systematic grid refinement study shows that the results are converged on the finest grid. The post-shock viscous dissipation is fully resolved, with $k_{\max}\eta \geq 1.7$ after the return to local isotropy in all cases. Thus the DNS databases are ideally suited for exploration of the fundamental physics and dynamics of shock/turbulence interaction.

It is argued that previous DNS studies of this problem may have been under-resolved in the post-shock region, since the Kolmogorov scale decreases during the interaction. A simple estimate of this change is given; it agrees with the DNS data to within 10%.

The present results show some qualitative differences with previous computations by Lee *et al.* (1993, 1997) and Jamme *et al.* (2002) and the linear interaction analysis (LIA) of Ribner (1954): the streamwise vorticity grows quickly and equilibrates with the transverse one; the Reynolds stresses are much more anisotropic; and this anisotropy persists at high Mach numbers (LIA predicts a reversal, which confirmed). The most plausible explanation for these differences is that nonlinear processes behind the shock are important, and that these processes were under-predicted in past computations (and obviously absent from the linear theory).

## ACKNOWLEDGMENTS

Financial support has been provided by the Department of Energy Scientific Discovery through Advanced Computing (SciDAC) program and the Natural Sciences and Engineering Research Council of Canada. The fine-grid calculations were run at the National Energy Research Scientific Computing Center under the ERCAP program.

### References

Barre, S., Alem, D. & Bonnet, J. P. 1996 Experimental study of a normal shock/homogeneous turbulence interaction. *AIAA J.* **34** (5), 968–974.

Ducros, F., Laporte, F., Souleres, T., Guinot, V., Moinat, P. & Caruelle, B. 2000 High-order fluxes for conservative skew-symmetric-like schemes in structured meshes: application to compressible flows. *J. Comput. Phys.* **161**, 114–139.

Jamme, S., Cazalbou, J.-B., Torres, F. & Chassaing, P. 2002 Direct numerical simulation of the interaction between a shock wave and various types of isotropic turbulence. *Flow, Turbulence and Combustion* **68**, 227–268.

Larsson, J. 2009 Blending technique for compressible inflow turbulence: algorithm localization and accuracy assessment. *J. Comput. Phys.* **228**, 933–937.

Larsson, J. & Gustafsson, B. 2008 Stability criteria for hybrid difference methods. *J. Comput. Phys.* **227**, 2886–2898.

Larsson, J., Lele, S. K. & Moin, P. 2007 Effect of numerical dissipation on the predicted spectra for compressible turbulence. In *Annual Research Briefs*, pp. 47–57. Center for Turbulence Research.

Lee, S., Lele, S. K. & Moin, P. 1993 Direct numerical simulation of isotropic turbulence interacting with a weak shock wave. *J. Fluid Mech.* **251**, 533–562.

Lee, S., Lele, S. K. & Moin, P. 1997 Interaction of isotropic turbulence with shock waves: effect of shock strength. *J. Fluid Mech.* **340**, 225–247.

Lele, S. K. 1992 Shock-jump relations in a turbulent flow. *Phys. Fluids* **4** (12), 2900–2905.

Mahesh, K., Lele, S. K. & Moin, P. 1997 The influence of entropy fluctuations on the interaction of turbulence with a shock wave. *J. Fluid Mech.* **334**, 353–379.

Pirozzoli, S. 2002 Conservative hybrid compact-WENO schemes for shock-turbulence interaction. *J. Comput. Phys.* **178**, 81–117.

Pope, S. B. 2000 *Turbulent Flows*. Cambridge University Press.

Ribner, H. S. 1954 Shock-turbulence interaction and the generation of noise. NACA Report 1233.

Ristorcelli, J. R. & Blaisdell, G. A. 1997 Consistent initial conditions for the DNS of compressible turbulence. *Phys. Fluids* **9** (1), 4–6.

Xiong, Z., Nagarajan, S. & Lele, S. K. 2004 Simple method for generating inflow turbulence. *AIAA J.* **42** (10), 2164–2166.